

## Novel MnWO<sub>x</sub> catalyst with remarkable performance for low temperature NH<sub>3</sub>-SCR of NO<sub>x</sub>†

Cite this: *Catal. Sci. Technol.*, 2013, **3**, 2699

Fudong Liu, Wenpo Shan, Zhihua Lian, Lijuan Xie, Weiwei Yang and Hong He\*

A novel W promoted MnO<sub>x</sub> catalyst (MnWO<sub>x</sub>) was used for the selective catalytic reduction (SCR) of NO<sub>x</sub> with NH<sub>3</sub> at low temperatures, with high deNO<sub>x</sub> efficiency from 60 to 250 °C under relatively high space velocity. The MnWO<sub>x</sub> catalyst showed a unique core-shell structure with Mn<sub>3</sub>O<sub>4</sub> covered by Mn<sub>5</sub>O<sub>8</sub> while Mn<sup>4+</sup> species at the outer surface served as a real active phase for NH<sub>3</sub>-SCR. The W doping resulted in the smaller particle size of MnO<sub>x</sub> active phase, increased the surface acidity and facilitated the NO/NH<sub>3</sub> oxidation, thus enhancing low temperature deNO<sub>x</sub> efficiency by promoting both Langmuir-Hinshelwood and Eley-Rideal reaction pathways. This novel catalyst is promising to be used in the deNO<sub>x</sub> process for flue gas after dust removal and desulfurization.

Received 10th May 2013,

Accepted 2nd July 2013

DOI: 10.1039/c3cy00326d

[www.rsc.org/catalysis](http://www.rsc.org/catalysis)

### 1. Introduction

NO<sub>x</sub> are major air pollutants endangering the eco-environment and human health, which are strictly controlled according to increasingly stringent legislation worldwide. Selective catalytic reduction of NO<sub>x</sub> with NH<sub>3</sub> (NH<sub>3</sub>-SCR) is a well established technique for the deNO<sub>x</sub> process of stationary sources at medium or high temperatures (>350 °C), using vanadium-based materials with biological toxicity as catalysts.<sup>1</sup> However, NH<sub>3</sub>-SCR of NO<sub>x</sub> at low temperatures (<250 °C) is still a challenging technique for the deNO<sub>x</sub> process of coal-fired power plants or other industrial boilers after desulfurization at low exhaust temperature.<sup>2</sup> For the purpose of energy conservation and emission reduction, low temperature NH<sub>3</sub>-SCR is worth studying and applying due to its high deNO<sub>x</sub> efficiency below 250 °C and convenience for installation of a catalytic converter without carrying out reconstruction of the present boilers. Therefore, the development of novel and efficient low temperature NH<sub>3</sub>-SCR catalysts is a research hotspot in environmental catalysis.

Among the reported vanadium-free catalysts, Mn-based catalysts (e.g. MnO<sub>x</sub>, MnO<sub>x</sub>/TiO<sub>2</sub>, MnO<sub>x</sub>-CeO<sub>x</sub> etc.) usually show excellent SCR activity even below 100 °C.<sup>3-9</sup> Compared to Fe or Cu modified zeolites such as Fe-ZSM-5,<sup>10-12</sup> Fe-BEA,<sup>13,14</sup> Cu-ZSM-5<sup>15</sup> and Cu-SSZ-13 catalysts<sup>16-18</sup> usually used in the deNO<sub>x</sub> process in diesel engines, the low temperature activity of Mn-based oxide catalysts is more advantageous to the application for NH<sub>3</sub>-SCR

of NO<sub>x</sub> from stationary sources, and the cost of using Mn-based oxide materials instead of zeolite materials is much lower. Tungsten is a commonly used promoter of SCR catalysts for stabilizing the active phase or supplying extra acid sites, such as for V<sub>2</sub>O<sub>5</sub>-WO<sub>3</sub>/TiO<sub>2</sub>,<sup>19</sup> CuO<sub>x</sub>/WO<sub>x</sub>-ZrO<sub>x</sub>,<sup>20,21</sup> CeO<sub>2</sub>-WO<sub>3</sub>/TiO<sub>2</sub><sup>22</sup> and CeWO<sub>x</sub><sup>23</sup> catalysts. Using a combination of the advantages of Mn species and W species, in this study, a novel MnWO<sub>x</sub> catalyst is reported for low temperature NH<sub>3</sub>-SCR reaction with high deNO<sub>x</sub> efficiency from 60 to 250 °C. The bulk and surface structures of this catalyst are characterized using different methods. The promotional effect of W species and the SCR reaction mechanism over the catalyst are discussed. The catalyst shows promise for low temperature deNO<sub>x</sub> of stationary flue gases after dust removal and deep desulfurization.

### 2. Experimental

#### 2.1 Catalyst preparation and activity test

Mn<sub>a</sub>W<sub>b</sub>O<sub>x</sub> catalysts (*a/b* = 2 : 1, 1 : 1 and 1 : 2) were prepared by a co-precipitation method using Mn(NO<sub>3</sub>)<sub>2</sub>, (NH<sub>4</sub>)<sub>6</sub>H<sub>2</sub>W<sub>12</sub>O<sub>40</sub>·5H<sub>2</sub>O as precursors and 25 wt% NH<sub>3</sub>·H<sub>2</sub>O as precipitator. First, a mixed aqueous solution of Mn(NO<sub>3</sub>)<sub>2</sub> and (NH<sub>4</sub>)<sub>6</sub>H<sub>2</sub>W<sub>12</sub>O<sub>40</sub>·5H<sub>2</sub>O with known concentrations using oxalic acid as the co-solvent was prepared. Then, 25 wt% NH<sub>3</sub>·H<sub>2</sub>O used as the precipitator was slowly added into the mixed solution until the pH rose to 10. Afterwards, the resulting precipitate was filtered, washed, dried at 100 °C for 12 h and finally calcined in air at 400 °C for 6 h. The pristine MnO<sub>x</sub> was prepared using the above-mentioned method, while the pristine WO<sub>x</sub> sample was obtained by direct decomposition of (NH<sub>4</sub>)<sub>6</sub>H<sub>2</sub>W<sub>12</sub>O<sub>40</sub>·5H<sub>2</sub>O in air at 600 °C for 3 h. After calcination, all powder samples were pressed, crushed and sieved to 40–60 mesh for activity test.

Research Center for Eco-Environmental Sciences, Chinese Academy of Sciences, 18 Shuangqing Road, Haidian District, Beijing 100085, P.R. China.

E-mail: honghe@rcees.ac.cn; Fax: +86 10 62849123; Tel: +86 10 62849123

† Electronic supplementary information (ESI) available: See DOI: 10.1039/c3cy00326d

The steady state  $\text{NH}_3$ -SCR and  $\text{NO}/\text{NH}_3$  oxidation activity over  $\text{Mn}_a\text{W}_b\text{O}_x$  catalysts was tested in a fixed-bed quartz tube reactor, and the reaction conditions were as follows: 40–60 mesh catalyst, catalyst volume of 0.6 ml (corresponding to 0.5–0.6 g catalyst by weight), 500 ppm  $\text{NO}$ , 500 ppm  $\text{NH}_3$ , 5 vol%  $\text{O}_2$ , 5 vol%  $\text{H}_2\text{O}$  (when used) and  $\text{N}_2$  balance; 500–2000  $\text{ml min}^{-1}$  flow rate and gas hourly space velocity (GHSV) of 50 000–200 000  $\text{h}^{-1}$ . The effluent gas including  $\text{NO}$ ,  $\text{NH}_3$ ,  $\text{N}_2\text{O}$  and  $\text{NO}_2$  was analyzed using an FTIR spectrometer (Nicolet Nexus 670) equipped with a low volume multiple-path gas cell (2 m). The  $\text{NO}_x$  conversion and  $\text{N}_2$  selectivity were calculated according to the formulas described in our previous study.<sup>24</sup>

## 2.2 Characterization

The  $\text{N}_2$  physisorption isotherms were measured at 77 K on a Quantachrome Quadrasorb SI-MP. Prior to  $\text{N}_2$  physisorption, the catalysts were degassed at 300 °C for 4 h. Surface areas were determined by BET equation in 0.05–0.35 partial pressure range. Pore volumes and average pore diameters were determined by BJH method from the desorption branches of isotherms.

The XRD measurements of  $\text{Mn}_a\text{W}_b\text{O}_x$  catalysts were carried out on PANalytical X'Pert Pro Diffractometer with  $\text{Cu K}\alpha$  radiation source ( $\lambda = 0.15406$  nm). The data of  $2\theta$  from 10 to 80° were collected at 8°  $\text{min}^{-1}$  with step size of 0.07°.

The XAFS of Mn-K edge in  $\text{Mn}_a\text{W}_b\text{O}_x$  catalysts were measured in transmission mode on a BL14W1 beamline, Shanghai Synchrotron Radiation Facility (SSRF) and BL-12C beamline, Photon Factory, KEK, Japan. Data were analyzed using IFEffit1.2.11.<sup>25</sup> XANES were normalized with edge height and then the first-order derivatives were taken to compare the variation of absorption edge energies. EXAFS oscillation  $\chi(k)$  was extracted using spline smoothing with a Cook–Sayers criterion,<sup>26</sup> and the filtered  $k^3$ -weighted  $\chi(k)$  was Fourier transformed into  $R$  space in the  $k$  range of 2.5–12  $\text{\AA}^{-1}$ . In the curve fitting step, the possible backscattering amplitude and phase shift were calculated using FEFF8.4.<sup>27</sup>

Raman spectra were collected at room temperature on a Spex 1877 D triplemate spectrograph with 2  $\text{cm}^{-1}$  resolution. A 532 nm DPSS diode-pump solid semiconductor laser was used as the excitation source with power output of ca. 30 mW.

TEM images of  $\text{MnO}_x$  and  $\text{MnWO}_x$  catalysts were obtained on an H-7500 Transmission Electron Microscopy (Hitachi) with 80 000 V and 400–500 k magnification.

The XPS of  $\text{Mn}_a\text{W}_b\text{O}_x$  catalysts was recorded on Scanning X-ray Microprobe (PHI Quantera, ULVAC-PHI, Inc.) using  $\text{Al K}\alpha$  radiation. Binding energies of Mn 2p and O 1s were calibrated using C 1s peak (BE = 284.8 eV).

The *in situ* DRIFTS were performed on an FTIR spectrometer (Nicolet Nexus 670) equipped with a smart collector and an MCT/A detector. The sample was pretreated at 400 °C for 0.5 h in 20 vol%  $\text{O}_2/\text{N}_2$  and then cooled down to 100 °C. The background spectrum was collected in flowing  $\text{N}_2$  and automatically subtracted from the sample spectrum. The reaction conditions were as follows: 500 ppm  $\text{NH}_3$ , 500 ppm  $\text{NO}$ , 5 vol%  $\text{O}_2$ ,  $\text{N}_2$  balance and 300  $\text{ml min}^{-1}$  flow rate. For each sample, the  $\text{NH}_3/(\text{NO} + \text{O}_2)$  adsorption time was controlled as 30 min.

Afterwards, the samples were purged by  $\text{N}_2$  for another 30 min until the infrared signals were stabilized. Finally,  $(\text{NO} + \text{O}_2)/\text{NH}_3$  was introduced into the gas chamber to react with the pre-adsorbed  $\text{NH}_3/\text{NO}_x$  species. All spectra were recorded by accumulating 100 scans with 4  $\text{cm}^{-1}$  resolution.

## 3. Results and discussion

### 3.1 $\text{NH}_3$ -SCR activity

As shown in Fig. 1, the pristine  $\text{MnO}_x$  prepared by a precipitation method only showed a narrow operation temperature window with over 80%  $\text{NO}_x$  conversion from 175 to 300 °C. When the Mn:W molar ratio was controlled at 2:1, the low temperature SCR activity was significantly enhanced with total  $\text{NO}_x$  conversion at 100 °C. Further increasing the Mn:W molar ratio to 1:1 resulted in the higher SCR activity at low temperatures, and the 100%  $\text{NO}_x$  conversion could be obtained at as low as 70 °C. Besides, the operation temperature window of  $\text{MnWO}_x$  catalyst was much wider than that of  $\text{MnO}_x$ , with the  $\text{NO}_x$  conversion above 80% from 60 to 250 °C. However, further increasing the Mn:W molar ratio to 1:2 led to the decline of low temperature SCR activity to a certain extent. Therefore, the optimal Mn:W molar ratio in  $\text{Mn}_a\text{W}_b\text{O}_x$  catalysts should be 1:1 in the preparation process. As for the pristine  $\text{WO}_x$ , there was no  $\text{NO}_x$  conversion observed at all over the whole temperature range, suggesting that the W species played only a role as catalyst promoter rather than active center for  $\text{NH}_3$ -SCR reaction. The  $\text{NH}_3$ -SCR activity results suggest that strong interaction between Mn and W species possibly exists in  $\text{Mn}_a\text{W}_b\text{O}_x$  catalysts in the preparation process and this effect is the strongest in the  $\text{MnWO}_x$  catalyst.

### 3.2 Influence of GHSV and $\text{H}_2\text{O}$

The  $\text{NH}_3$ -SCR activity over  $\text{MnWO}_x$  catalyst was also tested under different GHSVs. As shown in Fig. 2, the  $\text{NO}_x$  conversion at low temperatures decreased to a certain extent monotonically with the increase of GHSV from 50 000 to 200 000  $\text{h}^{-1}$ , yet the  $\text{NO}_x$  conversion above 200 °C was not obviously affected.

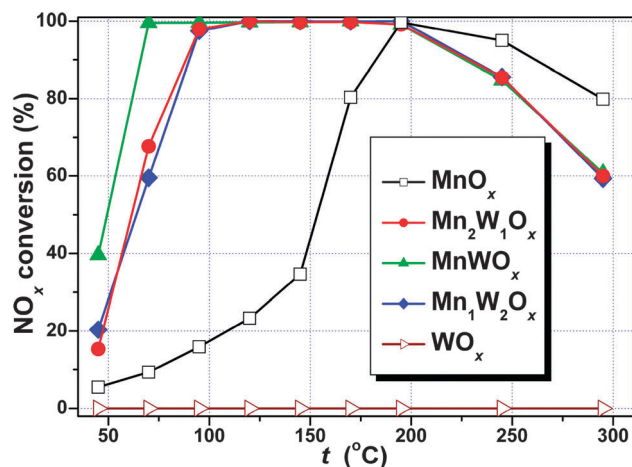


Fig. 1  $\text{NO}_x$  conversion over  $\text{Mn}_a\text{W}_b\text{O}_x$  catalysts in  $\text{NH}_3$ -SCR reaction at GHSV of 50 000  $\text{h}^{-1}$ .

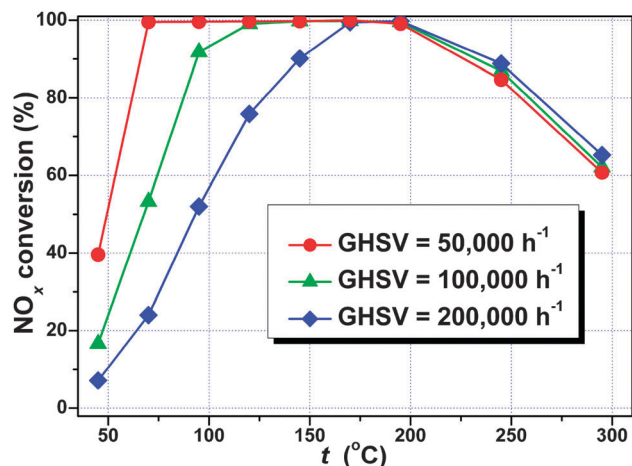


Fig. 2  $\text{NO}_x$  conversion over  $\text{MnWO}_x$  catalyst in  $\text{NH}_3$ -SCR reaction under different GHSVs.

Even under the GHSV of  $200\,000\text{ h}^{-1}$ , the  $\text{NO}_x$  conversion could still be maintained above 80% from 150 to 250 °C. In practical use, the high durability of this  $\text{MnWO}_x$  catalyst to space velocity is beneficial to reduce the volume of SCR catalytic converter for saving installation space. Furthermore, the stability tests in  $\text{NH}_3$ -SCR reaction (Fig. S1(A)†) showed that the  $\text{MnWO}_x$  catalyst is highly stable for  $\text{deNO}_x$  at low temperatures, which is also advantageous to the practical use.

After  $\text{deSO}_x$  using wet flue gas desulphurization (WFGD) method, the flue gas usually contains a certain fraction of water vapor, which may deactivate the SCR catalysts especially at low temperatures. For example, over  $\text{V}_2\text{O}_5/\text{AC}$ ,  $\text{MnO}_x/\text{Al}_2\text{O}_3$ ,  $\text{Fe}_{0.75}\text{Mn}_{0.25}\text{TiO}_x$  catalysts,<sup>28–30</sup> the inhibition effect of  $\text{H}_2\text{O}$  was clearly observed possibly due to the blocking of some active sites for activating  $\text{NH}_3$  or  $\text{NO}_x$ . As shown in Fig. 3, the presence of 5 vol%  $\text{H}_2\text{O}$  also showed apparent inhibition effect on  $\text{NH}_3$ -SCR activity of  $\text{MnWO}_x$  catalyst below 175 °C, with the temperature point achieving 100%  $\text{NO}_x$  conversion shifted *ca.* 100 °C towards high temperature range. However, comparing with the state-of-art

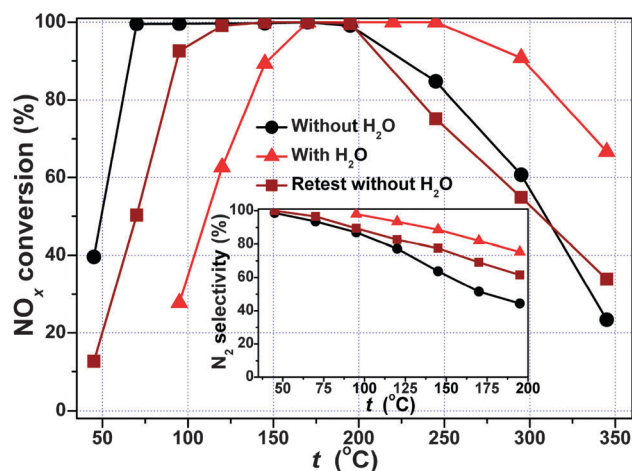


Fig. 3  $\text{NO}_x$  conversion over  $\text{MnWO}_x$  catalyst in  $\text{NH}_3$ -SCR reaction with/without 5 vol%  $\text{H}_2\text{O}$  at GHSV of  $50\,000\text{ h}^{-1}$  (inset:  $\text{N}_2$  selectivity).

$\text{NH}_3$ -SCR catalysts with excellent low temperature activity such as  $\text{Cu-ZSM-5}$ <sup>31,32</sup> and  $\text{Cu-SSZ-13}$ ,<sup>33,34</sup> the low temperature  $\text{deNO}_x$  efficiency from 100 to 200 °C over  $\text{MnWO}_x$  catalyst still showed some advantages in the presence of similar amount of  $\text{H}_2\text{O}$ . Besides, the presence of  $\text{H}_2\text{O}$  positively influenced the  $\text{N}_2$  selectivity over  $\text{MnWO}_x$  catalyst (inset Fig. 3). In the absence of  $\text{H}_2\text{O}$ , the  $\text{N}_2$  selectivity decreased sharply with increasing reaction temperature, which still needs to be improved in future studies by surface modification or promoter doping. In the presence of  $\text{H}_2\text{O}$ , the  $\text{N}_2$  selectivity was greatly enhanced, *e.g.* the  $\text{N}_2$  selectivity was increased from 60% to 90% at *ca.* 150 °C. This positive effect of  $\text{H}_2\text{O}$  on the  $\text{N}_2$  selectivity is attributed to inhibition of  $\text{NH}_3$  unselective oxidation by  $\text{H}_2\text{O}$  and is beneficial for practical use because  $\text{N}_2\text{O}$  is a potent greenhouse gas with restrictions placed on its emissions. Furthermore, as the results shown in Fig. S1(B),† even in the presence of water vapor, this  $\text{MnWO}_x$  catalyst can still have long term stability at 150 °C with a reversible deactivation effect by  $\text{H}_2\text{O}$ . However, after the  $\text{NH}_3$ -SCR activity test with  $\text{H}_2\text{O}$ , more ammonium nitrate species might form on the catalyst surface which could block some pores or active sites for  $\text{NH}_3/\text{NO}_x$  adsorption, resulting in a decrease in  $\text{NO}_x$  conversion below 125 °C over  $\text{MnWO}_x$  catalyst even after stopping the  $\text{H}_2\text{O}$  inlet (as shown in Fig. 3). Such phenomenon should be carefully considered for the practical use of this catalyst system.

### 3.3 NO oxidation and $\text{NH}_3$ oxidation

For low temperature  $\text{NH}_3$ -SCR, NO oxidation to  $\text{NO}_2$  is very important to promote  $\text{deNO}_x$  efficiency by accelerating the “fast SCR” process. If an SCR catalyst can produce  $\text{NO}_2$  *in situ* effectively under  $\text{NH}_3$ -SCR conditions, the low temperature SCR activity can be outstanding.<sup>35</sup> To understand in-depth the promotional effects of  $\text{WO}_x$  addition into  $\text{MnO}_x$ , separate NO oxidation experiments were carried out. As shown in Fig. 4A, the  $\text{WO}_x$  sample showed no NO oxidation activity over the whole temperature range, while the relatively higher NO conversion to  $\text{NO}_2$  could be achieved over  $\text{MnO}_x$ . Over the  $\text{MnWO}_x$  catalyst, much higher NO conversion to

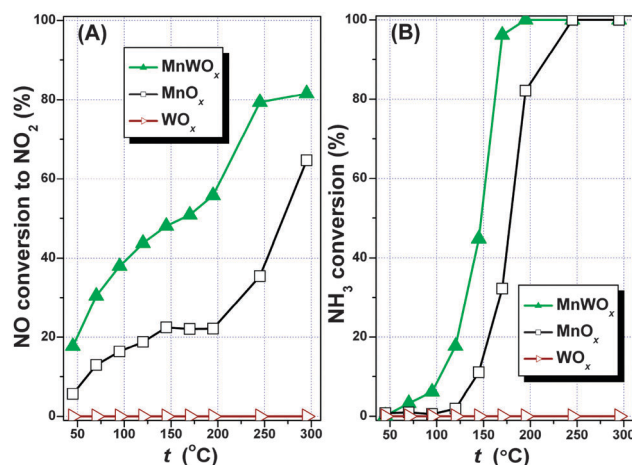


Fig. 4 (A) NO conversion and (B)  $\text{NH}_3$  conversion in separate NO and  $\text{NH}_3$  oxidation reactions over  $\text{MnWO}_x$ ,  $\text{MnO}_x$  and  $\text{WO}_x$  at GHSV of  $50\,000\text{ h}^{-1}$ .

NO<sub>2</sub> could be obtained than with MnO<sub>x</sub> over the whole temperature range (e.g. 50% vs. 20% at 150 °C), which is consistent with the SCR performance. These results clearly indicate that the enhancement of low temperature SCR activity of MnO<sub>x</sub> catalyst by WO<sub>x</sub> addition is strongly associated with facilitation of a “fast SCR” process.

For the promotion of low temperature activity of NH<sub>3</sub>-SCR catalyst, the activation of NH<sub>3</sub> at low temperatures is also very important. Therefore, separate NH<sub>3</sub> oxidation experiments were also carried out. As shown in Fig. 4B, the WO<sub>x</sub> sample showed no NH<sub>3</sub> oxidation activity over the whole temperature range. Over MnO<sub>x</sub> catalyst, the light-off temperature with 50% conversion for NH<sub>3</sub> oxidation was *ca.* 180 °C and the total conversion of NH<sub>3</sub> could be achieved at *ca.* 250 °C. After WO<sub>x</sub> doping, NH<sub>3</sub> oxidation activity of MnWO<sub>x</sub> catalyst was greatly enhanced, with the light-off temperature shifted to *ca.* 150 °C and the total conversion temperature shifted to *ca.* 200 °C. These results indicate that the W addition into MnO<sub>x</sub> can obviously enhance the activation of NH<sub>3</sub> or NH<sub>4</sub><sup>+</sup> adsorbed species on MnWO<sub>x</sub> catalyst surface and promote their reaction towards NO<sub>x</sub> to produce N<sub>2</sub>, which will be discussed in detail in the subsequent *in situ* DRIFTS experiments. Considering the reaction products from NH<sub>3</sub> oxidation over MnWO<sub>x</sub> catalyst, only the N<sub>2</sub>O by-product was detected (*i.e.* 65% selectivity to N<sub>2</sub> and 35% selectivity to N<sub>2</sub>O at 150 °C), indicating that the relatively low N<sub>2</sub> selectivity in NH<sub>3</sub>-SCR reaction over MnWO<sub>x</sub> catalyst might be partially owing to the unselective oxidation of NH<sub>3</sub>. In further study, the modification of this catalyst to inhibit the unselective NH<sub>3</sub> oxidation process would be an efficient way to improve the N<sub>2</sub> selectivity in NH<sub>3</sub>-SCR reaction.

### 3.4 N<sub>2</sub> physisorption

As shown in Table 1, for pristine MnO<sub>x</sub>, the corresponding textural parameters are as follows: BET surface area of 19.3 m<sup>2</sup> g<sup>-1</sup>, BJH desorption pore volume of 0.13 cm<sup>3</sup> g<sup>-1</sup> and BJH desorption pore diameter of 1.9 nm. The pristine WO<sub>x</sub> sample showed rather small surface area (0.01 m<sup>2</sup> g<sup>-1</sup>), pore volume (0.01 cm<sup>3</sup> g<sup>-1</sup>) and relatively larger pore diameter (2.5 nm). The doping of WO<sub>x</sub> into MnO<sub>x</sub> could significantly increase the surface area and pore volume of Mn<sub>a</sub>W<sub>b</sub>O<sub>x</sub> catalysts, and the pore diameter was also increased to a certain extent probably due to the formation of extra secondary piled pores. It is noteworthy that the MnWO<sub>x</sub> catalyst possessed the largest surface area (75.7 m<sup>2</sup> g<sup>-1</sup>) and pore volume (0.27 cm<sup>3</sup> g<sup>-1</sup>) possibly owing to the strongest interaction between Mn and W species in the preparation process, which is in good agreement with its highest NH<sub>3</sub>-SCR performance.

**Table 1** Structural parameters of Mn<sub>a</sub>W<sub>b</sub>O<sub>x</sub> catalysts derived from N<sub>2</sub> physisorption results

Samples	S <sub>BET</sub> [m <sup>2</sup> g <sup>-1</sup> ]	BJH desorption pore volume [cm <sup>3</sup> g <sup>-1</sup> ]	BJH desorption pore diameter [nm]
MnO <sub>x</sub>	19.3	0.13	1.9
Mn <sub>2</sub> W <sub>1</sub> O <sub>x</sub>	48.0	0.23	3.8
MnWO <sub>x</sub>	75.7	0.27	12.6
Mn <sub>1</sub> W <sub>2</sub> O <sub>x</sub>	53.2	0.26	12.5
WO <sub>x</sub>	0.01	0.01	2.5

Even after normalization, the NO<sub>x</sub> conversion per surface area over MnWO<sub>x</sub> catalyst is still higher than that over MnO<sub>x</sub>, Mn<sub>2</sub>W<sub>1</sub>O<sub>x</sub> and Mn<sub>1</sub>W<sub>2</sub>O<sub>x</sub> at 50 °C (*i.e.* 0.28, 0.32, 0.52 and 0.38% g m<sup>-2</sup> over MnO<sub>x</sub>, Mn<sub>2</sub>W<sub>1</sub>O<sub>x</sub>, MnWO<sub>x</sub> and Mn<sub>1</sub>W<sub>2</sub>O<sub>x</sub>, respectively), indicating that besides the increase of surface area by W doping, the interaction between Mn and W species is also important for the promotion of low temperature deNO<sub>x</sub> activity, which will be discussed later in the following sections.

### 3.5 Bulk structure characterized by XRD and XAFS

The pristine MnO<sub>x</sub>, as presented in Fig. 5, exhibited a mixed XRD pattern of Mn<sub>3</sub>O<sub>4</sub> and Mn<sub>5</sub>O<sub>8</sub>. It is noteworthy that the average valence of Mn species is *ca.* 2.67 in Mn<sub>3</sub>O<sub>4</sub> and *ca.* 3.2 in Mn<sub>5</sub>O<sub>8</sub>, therefore the Mn species in MnO<sub>x</sub> should have an intermediate average valence between 2.67 and 3.2. If this valence value could be determined by another method, the relative molar ratio of Mn<sub>3</sub>O<sub>4</sub> and Mn<sub>5</sub>O<sub>8</sub> could actually be calculated. After doping by WO<sub>x</sub>, the intensity of the diffraction peaks of Mn<sub>3</sub>O<sub>4</sub> and Mn<sub>5</sub>O<sub>8</sub> decreased obviously, indicating the smaller particle size of MnO<sub>x</sub>. For example, the full widths at half maximum (FWHMs) of (2, 0, 0) peak in Mn<sub>3</sub>O<sub>4</sub> at 2θ = *ca.* 18.0° for MnO<sub>x</sub>, Mn<sub>2</sub>W<sub>1</sub>O<sub>x</sub>, MnWO<sub>x</sub> and Mn<sub>1</sub>W<sub>2</sub>O<sub>x</sub> are 0.31, 0.43, 0.53 and 0.45, respectively, and the FWHMs of (2, 0, 1) peak in Mn<sub>5</sub>O<sub>8</sub> at 2θ = *ca.* 21.6° for corresponding samples are 0.23, 0.29, 0.50 and 0.40, respectively. These results indicate that the WO<sub>x</sub> species in Mn<sub>a</sub>W<sub>b</sub>O<sub>x</sub> catalysts showed a strong inhibition effect on the crystallization of the MnO<sub>x</sub> phase, which is beneficial to the increase of surface area plus pore volume, the decrease of pore diameter and thus the enhancement of SCR activity. For the WO<sub>x</sub> sample, only a well crystallized WO<sub>3</sub> phase with sharp and intense diffraction peaks was observed.

The XAFS of Mn-K edge were measured using Mn foil, MnO, Mn<sub>3</sub>O<sub>4</sub>, Mn<sub>2</sub>O<sub>3</sub> and MnO<sub>2</sub> as reference samples. As shown in Fig. 6A, not only the pre-edge peaks but also the post-edge regions of Mn-K XANES in Mn<sub>a</sub>W<sub>b</sub>O<sub>x</sub> catalysts were quite similar to that in MnO<sub>x</sub>. These results imply that although the particle size of MnO<sub>x</sub> phase judged from XRD results was obviously decreased after WO<sub>x</sub> doping, the crystal structure of Mn<sub>a</sub>W<sub>b</sub>O<sub>x</sub> catalysts remained unchanged. Due to the mixture state of Mn species in MnO<sub>x</sub> and

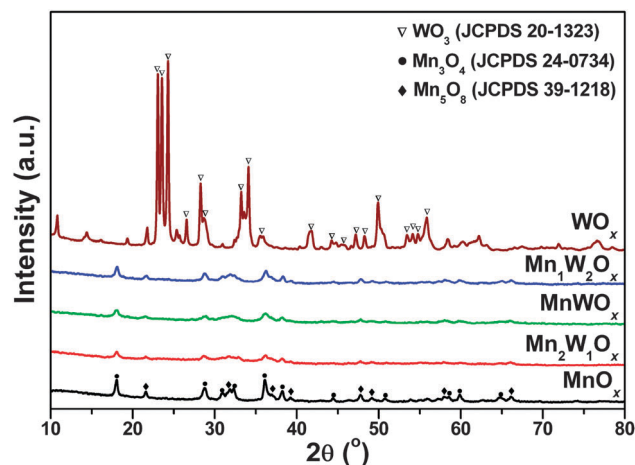


**Fig. 5** Power XRD of Mn<sub>a</sub>W<sub>b</sub>O<sub>x</sub> catalysts.

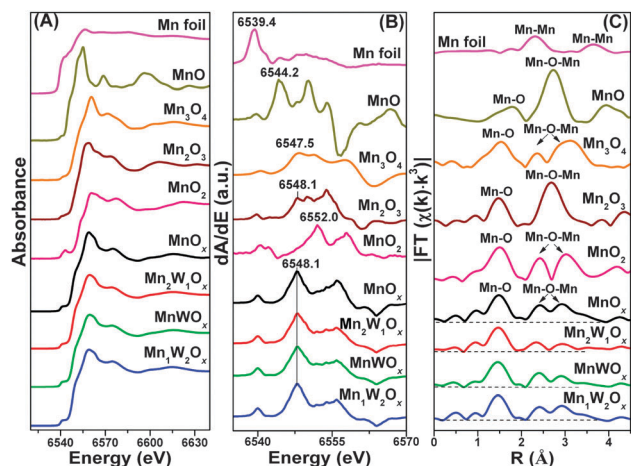


**Fig. 6** (A) XANES, (B) first-order derivatives of XANES and (C) Fourier transformed filtered  $k^3$ -weighted EXAFS oscillations of Mn-K edge in  $Mn_aW_bO_x$  catalysts.

$Mn_aW_bO_x$  catalysts (*i.e.*  $Mn_3O_4$  and  $Mn_5O_8$ ), all the catalysts showed discrepant XANES patterns compared to the reference samples. To further determine the average valence of Mn species in  $Mn_aW_bO_x$  catalysts, the first-order derivatives of Mn-K XANES were taken. As shown in Fig. 6B, the absorption edge energy of Mn species (*i.e.* the corresponding energy relative to the maximum of first-order derivatives) in  $Mn_aW_bO_x$  catalysts was 6548.1 eV, which was identical to that in  $Mn_2O_3$  reference. Therefore, the average valence of Mn species in  $Mn_aW_bO_x$  catalysts is +3, based on which the molar ratio of  $Mn_3O_4$  and  $Mn_5O_8$  can be calculated as 1 : 1.

Fig. 6C shows the Fourier transformed filtered  $k^3$ -weighted EXAFS oscillations into  $R$  space of Mn-K edge, and Table 2 shows the curve fitting results. Also due to the mixture state of Mn species in  $Mn_aW_bO_x$  catalysts, the coordination shells of Mn-O and Mn-O-Mn in our catalysts were different to a certain extent when compared with the reference samples. Generally, the peak intensity of the second coordination shells in metal oxides can be used as a crystallinity indicator of target materials. The lower peak intensity of the second coordination shells,

**Table 2** Curve fitting results of Mn K-edge EXAFS in  $Mn_aW_bO_x$  catalysts

Sample	Shell	CN <sup>a</sup>	$R^b$ (Å)	DW <sup>c</sup> (Å)	$R$ factor (%)
$MnO_x$	Mn-O	4.3	1.91	0.054	4.7
	Mn-Mn <sub>1</sub>	3.1	2.82	0.069	
	Mn-Mn <sub>2</sub>	3.1	3.45	0.009	
$Mn_2W_1O_x$	Mn-O	4.1	1.90	0.063	3.3
	Mn-Mn <sub>1</sub>	2.8	2.82	0.095	
	Mn-Mn <sub>2</sub>	2.3	3.45	0.069	
$MnWO_x$	Mn-O	3.8	1.89	0.054	2.4
	Mn-Mn <sub>1</sub>	2.5	2.82	0.070	
	Mn-Mn <sub>2</sub>	1.7	3.45	0.014	
$Mn_1W_2O_x$	Mn-O	3.8	1.90	0.055	1.5
	Mn-Mn <sub>1</sub>	3.1	2.82	0.076	
	Mn-Mn <sub>2</sub>	2.3	3.44	0.010	

<sup>a</sup> CN: coordination number. <sup>b</sup>  $R$ : bond distance. <sup>c</sup> DW: Debye-Waller factor.

the poorer crystallization degree of the sample. Accordingly, it is obvious that the  $MnO_x$  sample showed much poorer crystallization degree than the Mn-containing references, with more unsaturated catalytically active sites. After curve fitting, the  $MnO_x$  sample was confirmed to possess Mn-O, Mn-O-Mn<sub>1</sub> and Mn-O-Mn<sub>2</sub> coordination shells at *ca.* 1.91, 2.82 and 3.45 Å with the coordination numbers being 4.3, 3.1, and 3.1, respectively. The introduction of W species into  $MnO_x$  further lowered the peak intensity of Mn-O-Mn coordination shells, and the coordination numbers of Mn-O-Mn<sub>1</sub> and Mn-O-Mn<sub>2</sub> in  $Mn_aW_bO_x$  catalysts were correspondingly decreased to a certain extent, confirming again the inhibition effect of  $WO_x$  on the crystallization of  $MnO_x$  phase. The  $MnWO_x$  catalyst with the best  $NH_3$ -SCR performance showed the smallest coordination numbers for Mn-O-Mn, suggesting that this catalyst possessed the most abundant surface defects, which was beneficial to the adsorption and activation of reactants for the de $NO_x$  process.

### 3.6 Surface structure characterized by Raman spectra and XPS

Comparing with XRD and XAFS, the Raman spectra and XPS are more surface sensitive for the characterization of  $Mn_aW_bO_x$  catalysts. As shown in Fig. 7, pristine  $MnO_x$  presented typical Raman shifts ascribed to  $Mn_5O_8$  ( $A_g$  mode at 647  $cm^{-1}$ , and non-assignable Raman-active modes at 267, 478, 537, 578, 617  $cm^{-1}$ ),<sup>36,37</sup> while no bands attributed to  $Mn_3O_4$  were observed, indicating that the  $MnO_x$  probably exhibits a core-shell structure with the  $Mn_3O_4$  phase covered by  $Mn_5O_8$  phase. The W addition into  $MnO_x$  decreased the band intensity to a certain extent, suggesting a smaller particle size of  $Mn_5O_8$  on surface layers. Besides, no Raman shifts ascribed to  $WO_3$  were observed for  $Mn_aW_bO_x$  catalysts, such as W-O-W bending modes at 272, 323  $cm^{-1}$  ( $F_{2g}$ ), W-O stretching mode at 719  $cm^{-1}$  ( $A_{1g}$ ) and W-O bending mode at 819  $cm^{-1}$  ( $E_g$ ).<sup>38-40</sup> These results combined with XRD results clearly suggest that the W species in  $Mn_aW_bO_x$  catalysts is mainly present in a highly dispersed state. To better confirm the formation of core-shell structure in  $MnO_x$  and  $MnWO_x$  catalysts, the TEM images were measured and the results are shown in Fig. 8. As we can clearly see, both  $MnO_x$  and  $MnWO_x$

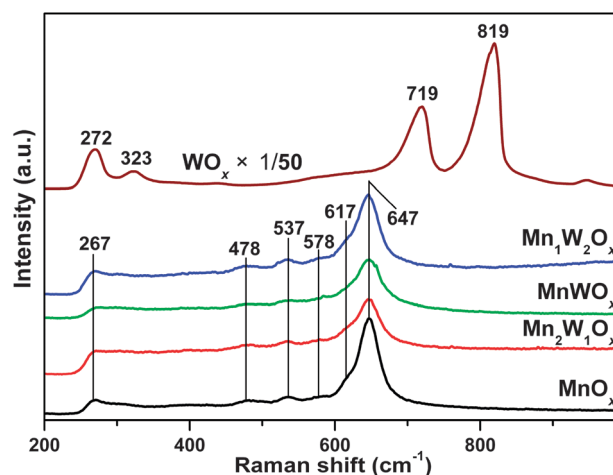


**Fig. 7** Raman spectra of  $Mn_aW_bO_x$  catalysts.

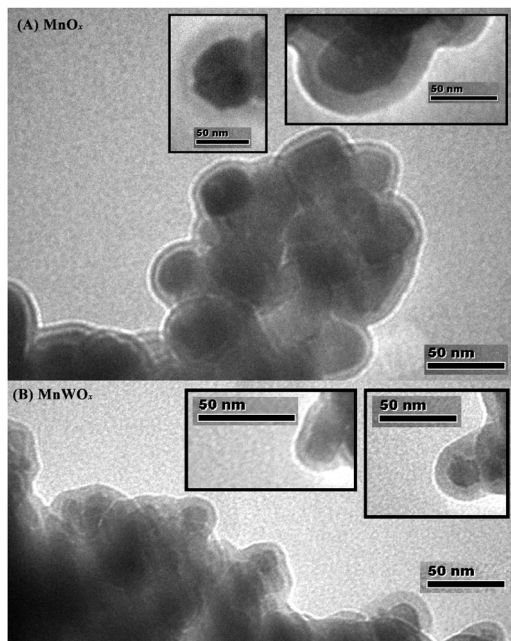


Fig. 8 TEM images of (A)  $\text{MnO}_x$  and (B)  $\text{MnWO}_x$  catalysts.

catalysts exhibited unique core-shell structures with legible cores and shells with relatively high and low density, respectively, and the  $\text{MnWO}_x$  catalyst possessed much smaller particle size than pristine  $\text{MnO}_x$  sample, which are totally in good agreement with the conclusions drawn from XRD, XAFS and Raman spectra results as we mentioned above.

As shown in Fig. 9A, two XPS bands of Mn 2p at *ca.* 642.1 and 653.6 eV were observed for  $\text{MnO}_x$ , corresponding to the photoelectron peaks of Mn 2p<sub>3/2</sub> and Mn 2p<sub>1/2</sub>, respectively. These binding energies are quite close to those of Mn 2p<sub>3/2</sub> and Mn 2p<sub>1/2</sub> on  $\text{MnO}_2$ , in which the Mn species is in the valence state of +4.<sup>7,41</sup> It is reported that  $\text{Mn}_5\text{O}_8$  (with compositional formula  $\text{Mn}_2^{2+}\text{Mn}_3^{4+}\text{O}_8$ ) is probably the only binary Mn oxide that is known to have a layered structure, in which the 2D octahedral sheets of  $[\text{Mn}_3^{4+}\text{O}_8]^{4-}$  consisting of  $\text{Mn}^{4+}$  ions are separated by

$\text{Mn}^{2+}$  layers and the outer surfaces are mainly composed of  $\text{Mn}^{4+}$  species.<sup>36</sup> Therefore, it is reasonable to deduce that the apparent valence of Mn species on  $\text{MnO}_x$  detected by XPS was close to that of  $\text{MnO}_2$ , higher than the ideal value of  $\text{Mn}_5\text{O}_8$  (+3.2). To better confirm this point of view, the Mn 2p XPS peaks were deconvoluted by searching for the optimal combination of Gaussian sub-bands with correlation coefficients ( $r^2$ ) above 0.99 using PeakFit4.12. As we can clearly see, besides the  $\text{Mn}^{2+}$  species with Mn 2p<sub>3/2</sub> peak at 641.5 eV and Mn 2p<sub>1/2</sub> peak at 653.1 eV along with some  $\text{Mn}^{7+}$  species (probably manganese nitrate and some other high-valent  $\text{Mn}^{6+/7+}$  species) with Mn 2p<sub>3/2</sub> peak in the range of 645.3–646.1 eV and Mn 2p<sub>1/2</sub> peak in the range of 655.2–657.1 eV, the dominant Mn species on the catalyst surface was indeed  $\text{Mn}^{4+}$  with Mn 2p<sub>3/2</sub> peak at 642.1 eV and Mn 2p<sub>1/2</sub> peak at 653.6 eV.<sup>7</sup> In other words, the main Mn species active for  $\text{NH}_3$ -SCR in this study was in the valence state of +4, similar as the conclusion drawn by Thirupathi and Smirniotis on their Mn–Ni/TiO<sub>2</sub> catalysts,<sup>7</sup> while the  $\text{Mn}^{2+}$  species in  $\text{Mn}_5\text{O}_8$  and the inner  $\text{Mn}_3\text{O}_4$  phase were possibly only present as “spectator components”. Under  $\text{NH}_3$ -SCR atmosphere, the  $\text{Mn}^{4+}$  species on outer surface might participate into the redox process between  $\text{Mn}^{4+}$  and  $\text{Mn}^{3+}$  for the activation of  $\text{NH}_3$  or  $\text{NO}_x$ . After W doping, the photoelectron peaks of Mn 2p showed some increase in intensity suggesting the higher surface concentration of  $\text{Mn}^{4+}$  species induced by smaller particle size of  $\text{MnO}_x$ , which is in good agreement with the Raman spectra. Based on the deconvolution results in this study and the calculation method from Thirupathi and Smirniotis’s work,<sup>7</sup> the  $\text{Mn}^{4+}/\text{Mn}^{2+}$  surface atomic ratios were calculated to be 3.2, 5.2, 7.1 and 5.1 for  $\text{MnO}_x$ ,  $\text{Mn}_2\text{W}_1\text{O}_x$ ,  $\text{MnWO}_x$  and  $\text{Mn}_1\text{W}_2\text{O}_x$ , respectively, and the percentages of  $\text{Mn}^{4+}/(\text{Mn}^{4+} + \text{Mn}^{2+})$  were correspondingly calculated to be 76%, 84%, 88% and 84%. The  $\text{MnWO}_x$  catalyst with the best  $\text{NH}_3$ -SCR performance possessed the highest surface concentration of  $\text{Mn}^{4+}$  species, which is also in good agreement with the conclusion drawn by Thirupathi and Smirniotis.<sup>7</sup>

As we stated in the experimental section, the Mn precursor was  $\text{Mn}(\text{NO}_3)_2$  in which the Mn species was mainly in the valence state of 2+. After precipitation at higher pH value, we believe that the precipitates mainly contained  $\text{Mn}(\text{OH})_x$  in which the  $\text{Mn}^{2+}$  species was still dominant. After desiccation and calcination in air conditions, the  $\text{Mn}^{2+}$  species in outer layers of  $\text{Mn}(\text{OH})_x$  could be transformed into  $\text{Mn}^{3+}$  and  $\text{Mn}^{4+}$  species easily under an oxidizing atmosphere (resulting in the formation of above-mentioned  $\text{Mn}_5\text{O}_8$ ), and the  $\text{Mn}^{2+}$  species in inner layers of  $\text{Mn}(\text{OH})_x$  could only be oxidized to  $\text{Mn}^{3+}$  species partially due to the limitation of oxygen diffusion (resulting in the formation of above-mentioned  $\text{Mn}_3\text{O}_4$ ). Thus, the core-shell structure of  $\text{MnO}_x$  with  $\text{Mn}_3\text{O}_4$  as core and  $\text{Mn}_5\text{O}_8$  as shell was formed. In the preparation process, the addition of W species could well inhibit the growth of  $\text{MnO}_x$  into large particles, leaving more Mn species to be oxidized in outer layers. Therefore, it is reasonable to obtain higher surface concentration of  $\text{Mn}^{4+}$  species on the W promoted  $\text{MnWO}_x$  catalyst than that on the pristine  $\text{MnO}_x$  sample, which is beneficial to the improvement of  $\text{NO}$  oxidation ability and thus low temperature  $\text{NH}_3$ -SCR activity.

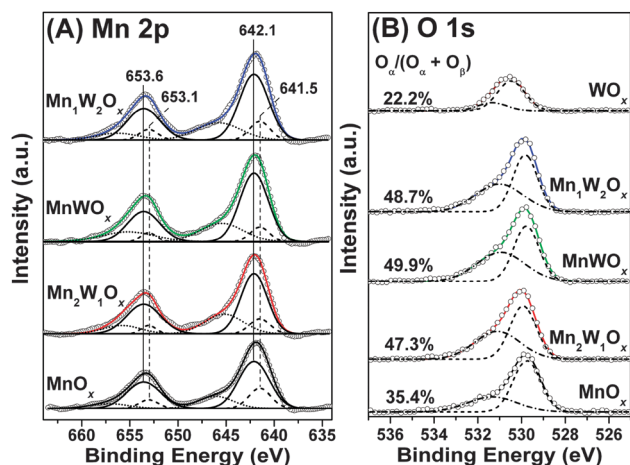


Fig. 9 XPS of (A) Mn 2p and (B) O 1s on  $\text{Mn}_n\text{W}_b\text{O}_x$  catalysts.

The O 1s XPS of  $Mn_aW_bO_x$  catalysts after deconvolution are shown in Fig. 9B. The sub-bands at lower binding energy (529.7–530.4 eV) corresponded to the lattice oxygen  $O^{2-}$  (denoted as  $O_\beta$ ), and the sub-bands at higher binding energy (531.0–531.3 eV) corresponded to the surface adsorbed oxygen (denoted as  $O_\alpha$ ), such as  $O_2^{2-}$  or  $O^-$  belonging to defect-oxide or hydroxyl-like group.<sup>42</sup> Generally,  $O_\alpha$  is more reactive in oxidation reactions due to its higher mobility than  $O_\beta$ ,<sup>3</sup> which is also beneficial to the NO oxidation to  $NO_2$  thus facilitating the “fast SCR” process. Therefore, the ratios of  $O_\alpha/(O_\alpha + O_\beta)$  on all samples are calculated and listed. As we can see, the W addition into  $MnO_x$  greatly increased the  $O_\alpha/(O_\alpha + O_\beta)$  ratio, e.g. the ratio was as high as 49.9% for  $MnWO_x$  catalyst. Much more amount of surface adsorbed oxygen was observed on  $MnWO_x$  catalyst than those on pristine  $MnO_x$  (35.4%) and  $WO_x$  (22.2%), indicating that the strong interaction between Mn and W species could produce extra surface vacancies to activate oxygen and also more surface hydroxyls participating into the SCR reaction.

### 3.7 In situ DRIFTS

To investigate the influence of W addition on  $NH_3/NO_x$  adsorption together with the SCR reaction mechanism, *in situ* DRIFTS were conducted at 100 °C and the results are shown in Fig. 10. After  $NH_3$  adsorption and  $N_2$  purge (Fig. 10A), no bands attributed to adsorbed  $NH_3$  species were detected on  $WO_x$ , probably due to its very small surface area. In contrast, on the  $MnO_x$  sample, the bands attributed to coordinated  $NH_3$  ( $\delta_{as}$  at 1603  $cm^{-1}$ ,  $\delta_s$  at 1188  $cm^{-1}$  and N–H stretching vibration modes at 3346, 3244, 3155  $cm^{-1}$ ) bound to Lewis acid sites<sup>43,44</sup> were clearly observed. Besides, a small amount of ionic  $NH_4^+$  species bound to Brønsted acid sites ( $\delta_{as}$  at 1450  $cm^{-1}$ ) was also formed,<sup>43,45</sup> along with the formation of consumption bands of surface acidic hydroxyls at 3593 and 3442  $cm^{-1}$ .<sup>46,47</sup> It is noteworthy that the amide species ( $-NH_2$ ) resulting from dehydrogenation of adsorbed  $NH_3$  was also detected (1558  $cm^{-1}$ ),<sup>47</sup> which can react directly with gaseous or weakly adsorbed NO to form  $NH_2NO$  and then decompose into  $N_2$  and  $H_2O$ . After W addition,

the band intensities of adsorbed  $NH_3$  species bound to both Lewis and Brønsted acid sites (including the  $\delta_s$  vibration mode of  $NH_4^+$  at 1684  $cm^{-1}$ ) together with the  $-NH_2$  species on  $MnWO_x$  catalyst were greatly enhanced, indicating a higher surface acidity and oxidation ability induced by W species. Another shoulder band at 1419  $cm^{-1}$  possibly ascribed to  $NH_4^+$  bound to W sites was also observed,<sup>48</sup> indicating that the doped W species can play a role as extra Brønsted acid sites on  $MnWO_x$  catalyst surface.

After NO +  $O_2$  adsorption and  $N_2$  purge (Fig. 10B), on  $WO_x$  sample, no bands ascribed to either nitrite or nitrate species were observed. In contrast, on the  $MnO_x$  sample, several distinct infrared bands attributed to monodentate nitrate ( $\nu_3$  high at 1524  $cm^{-1}$  and  $\nu_3$  low 1271  $cm^{-1}$ ), bridging nitrate ( $\nu_3$  high at 1626  $cm^{-1}$ ) and bidentate nitrate ( $\nu_3$  high at 1593  $cm^{-1}$  and  $\nu_1$  at 1011  $cm^{-1}$ )<sup>49–52</sup> were clearly present. The negative bands attributed to the consumption of surface basic hydroxyls through interaction with  $NO_x$  were also observed at 3631 and 3585  $cm^{-1}$ ,<sup>53</sup> which were different from those ascribed to the surface acidic hydroxyls in Fig. 10A. After W addition, the adsorbed nitrate species showed an obvious increase in intensity, especially the monodentate nitrate. In our previous study, we concluded that the reactivity of monodentate nitrate in SCR reaction was much higher than that of bridging nitrate, while bidentate nitrate was only present as spectator species.<sup>54,55</sup> Therefore, the enhanced formation of monodentate nitrate on the W promoted catalyst is evidently responsible for the improvement of low temperature  $NH_3$ -SCR activity.

To confirm the reactivity of adsorbed  $NH_3$  species in SCR reaction on  $MnWO_x$  catalyst, the *in situ* DRIFTS of reaction between pre-adsorbed  $NH_3$  and NO +  $O_2$  were recorded as a function of time (Fig. 10C). After the introduction of NO +  $O_2$  at 100 °C, the adsorbed  $NH_3$  species including coordinated  $NH_3$  (1603 and 1192  $cm^{-1}$ ), ionic  $NH_4^+$  (1684, 1450 and 1419  $cm^{-1}$ ) and  $-NH_2$  species (1558  $cm^{-1}$ ) showed an apparent decrease in intensity due to the reaction with  $NO_x$ , indicating that both Lewis and Brønsted acid sites on  $MnWO_x$  catalyst contribute to the SCR reaction and the reaction between  $-NH_2$  and NO through Eley–Rideal (E–R) mechanism can proceed at low temperature. At the same time, the surface acidic hydroxyl groups (3593 and 3442  $cm^{-1}$ ) were liberated owing to the consumption of ionic  $NH_4^+$ , while the basic hydroxyl groups (3631 and 3585  $cm^{-1}$ ) were consumed by  $NO_x$  adsorption with the formation of monodentate nitrate (1525 and 1275  $cm^{-1}$ ), bridging nitrate (1626  $cm^{-1}$ ) and bidentate nitrate (1593 and 1012  $cm^{-1}$ ). It is noteworthy that after the introduction of NO +  $O_2$  for 2 or 3 min, two shoulder bands at 1456 and 1290  $cm^{-1}$  can be hazily observed, which might be a reactive intermediate species in  $NH_3$ -SCR reaction.

In contrast, the reactivity of adsorbed  $NO_x$  species in SCR reaction on  $MnWO_x$  catalyst was also investigated by *in situ* DRIFTS of reaction between pre-adsorbed  $NO_x$  and  $NH_3$  as a function of time (Fig. 10D). After the introduction of  $NH_3$ , both monodentate nitrate (1524 and 1271  $cm^{-1}$ ) and bridging nitrate (1626  $cm^{-1}$ ) showed a rapid decrease in intensity, indicating that these nitrate species were reactive in the SCR reaction.

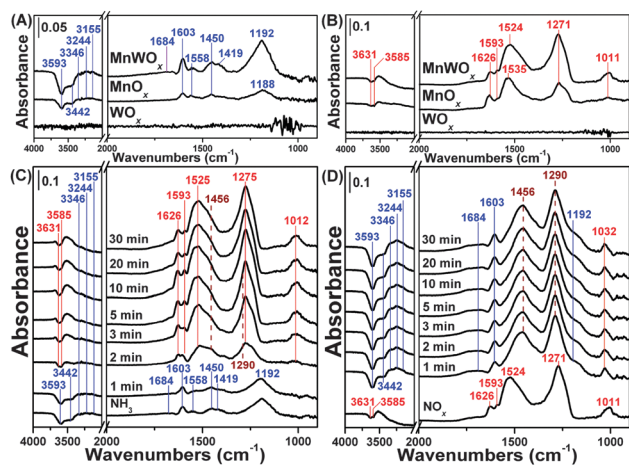


**Fig. 10** *In situ* DRIFTS of (A)  $NH_3$  adsorption, (B) NO +  $O_2$  adsorption at 100 °C on  $MnWO_x$ ,  $MnO_x$  and  $WO_x$ , (C) NO +  $O_2$  reacted with pre-adsorbed  $NH_3$  species, and (D)  $NH_3$  reacted with pre-adsorbed  $NO_x$  species at 100 °C on  $MnWO_x$ .

At the same time, the bands attributed to coordinated  $\text{NH}_3$  (1603 and  $1192\text{ cm}^{-1}$ ) and ionic  $\text{NH}_4^+$  ( $1684\text{ cm}^{-1}$ ) were observed, and the band positions of the consumed surface basic hydroxyls also shifted to those corresponding to acidic hydroxyls. Although the  $\nu_3$  high vibration mode of bidentate nitrate at  $1593\text{ cm}^{-1}$  might be overlapped by the growing bands at 1603 and  $1456\text{ cm}^{-1}$ , we can still confirm its presence through the  $\nu_1$  vibration mode at  $1032\text{ cm}^{-1}$ . The blue shift of this band might be caused by the interaction between bidentate nitrate and adsorbed  $\text{NH}_3$  species. It is noticeable that two distinct bands at 1456 and  $1290\text{ cm}^{-1}$  were clearly observed, which cannot be ascribed only to either adsorbed  $\text{NH}_3$  or adsorbed  $\text{NO}_x$  species. In our previous study,<sup>30</sup> these intermediate species were also observed, which was confirmed to be surface ammonium nitrate ( $\text{NH}_4\text{NO}_3$ ) originating from  $\text{NO}_2$  dimerization, disproportionate in the presence of  $\text{H}_2\text{O}$  and successive reaction with  $\text{NH}_3$ .<sup>56–58</sup> Besides, the reactivity of surface  $\text{NH}_4\text{NO}_3$  in SCR reaction was also verified,<sup>30</sup> following the equations as follows:  $\text{NH}_4\text{NO}_3 + \text{NO} \rightarrow \text{NH}_4\text{NO}_2 + \text{NO}_2$ ,  $\text{NH}_4\text{NO}_2 \rightarrow \text{N}_2 + 2\text{H}_2\text{O}$ . The importance of surface  $\text{NH}_4\text{NO}_3$  species in SCR reaction and the similar Langmuir–Hinshelwood (L–H) reaction mechanism were also observed by other researchers over  $\text{V}_2\text{O}_5\text{--WO}_3/\text{TiO}_2$ , Fe-ZSM-5 and Cu-ZSM-5 catalysts.<sup>56,59–61</sup> From *in situ* DRIFTS results we can conclude that, the SCR reaction at low temperatures over  $\text{MnWO}_x$  catalyst follows both L–H mechanism between  $\text{NH}_3$  adsorbed species and nitrate species plus E–R mechanism between  $-\text{NH}_2$  species and gaseous NO. The W addition into  $\text{MnO}_x$  results in higher adsorption ability of  $\text{NH}_3$  and  $\text{NO}_x$  simultaneously, thus promoting the L–H reaction pathway; the oxidation ability of W doped catalyst is also enhanced with higher surface concentration of  $-\text{NH}_2$  species formed after  $\text{NH}_3$  adsorption, thus promoting the E–R reaction pathway. Besides, as presented in Fig. 4, the NO oxidation over  $\text{MnWO}_x$  catalyst lighted-off at much lower temperatures than the  $\text{NH}_3$  oxidation (*e.g.* the NO conversion to  $\text{NO}_2$  was *ca.* 40% at  $100\text{ }^\circ\text{C}$  whereas the  $\text{NH}_3$  conversion was *ca.* 10%), and these data indicate that the L–H mechanism is probably more important at low temperatures.

It should be noted that if in the presence of water vapor, the transformation of partial Lewis acid sites into Brønsted acid sites might occur due to the hydroxylation effect, and the  $\text{NH}_3$  adsorption as  $\text{NH}_4^+$  species was enhanced to a certain extent, as confirmed by the DRIFTS results in Fig. S2(A).<sup>†</sup> However, at the same time, the  $\text{NO}_x$  adsorption might be inhibited to a certain extent, as verified by the DRIFTS results in Fig. S2(B),<sup>†</sup> thus resulting in the partial inhibition of L–H reaction pathway and the decrease of low temperature  $\text{NH}_3$ -SCR activity in the presence of  $\text{H}_2\text{O}$ . After the stop of  $\text{H}_2\text{O}$ , both the  $\text{NH}_3$  and  $\text{NO}_x$  adsorption over  $\text{MnWO}_x$  catalyst could be recovered to the initial status, indicating that this inhibition effect of  $\text{H}_2\text{O}$  at short time was reversible. Under the  $\text{NH}_3$ -SCR reaction atmosphere, the ammonium nitrate species could form on the catalyst surface, as shown by the DRIFTS results in Fig. S2(C),<sup>†</sup> and its deposition amount would be increased gradually in the presence of  $\text{H}_2\text{O}$  if operating at long term. The severe deposition of ammonium nitrate on catalyst surface would lead to the blocking of pore

channels and the occupation of active sites, thus resulting in the decline of low temperature de $\text{NO}_x$  efficiency to a certain extent. In practical use, the regeneration strategy such as steam washing or periodic heating can be applied to reduce this deactivation problem.

## 4. Conclusions

A novel W promoted  $\text{MnO}_x$  catalyst was used for  $\text{NH}_3$ -SCR of  $\text{NO}_x$  at low temperatures, which showed high de $\text{NO}_x$  efficiency from 60 to  $250\text{ }^\circ\text{C}$ . The  $\text{MnWO}_x$  catalyst exhibited a core-shell structure, with the  $\text{Mn}_3\text{O}_4$  phase covered by  $\text{Mn}_5\text{O}_8$  possessing high concentration of  $\text{Mn}^{4+}$  species at outer surfaces. The W addition decreased the particle size of  $\text{MnO}_x$  phase, increased the surface acidity and facilitated the NO/ $\text{NH}_3$  oxidation, thus improving the low temperature  $\text{NH}_3$ -SCR activity by promoting both L–H and E–R reaction pathways.

## Acknowledgements

This work was supported by the National Natural Science Foundation of China (51108446, 51221892), the Ministry of Science and Technology, China (2012AA062506), BL14W1 beamline, SSRF and Photon Factory, KEK, Japan (2012G537). The authors would also like to thank the help from Prof. Kiyotaka Asakura for XAFS experiments and Dr Lian Wang for measuring TEM images.

## Notes and references

- 1 G. Busca, L. Lietti, G. Ramis and F. Berti, *Appl. Catal., B*, 1998, **18**, 1.
- 2 J. Li, H. Chang, L. Ma, J. Hao and R. T. Yang, *Catal. Today*, 2011, **175**, 147.
- 3 Z. Wu, R. Jin, Y. Liu and H. Wang, *Catal. Commun.*, 2008, **9**, 2217.
- 4 B. Thirupathi and P. Smirniotis, *Catal. Lett.*, 2011, **141**, 1399.
- 5 X. Tang, J. Hao, W. Xu and J. Li, *Catal. Commun.*, 2007, **8**, 329.
- 6 F. Eigenmann, M. Maciejewski and A. Baiker, *Appl. Catal., B*, 2006, **62**, 311.
- 7 B. Thirupathi and P. G. Smirniotis, *J. Catal.*, 2012, **288**, 74.
- 8 P. R. Ettireddy, N. Ettireddy, T. Boningari, R. Pardemann and P. G. Smirniotis, *J. Catal.*, 2012, **292**, 53.
- 9 A. Sultana, M. Sasaki and H. Hamada, *Catal. Today*, 2012, **185**, 284.
- 10 M. Schwidder, S. Heikens, A. De Toni, S. Geisler, M. Berndt, A. Brückner and W. Grünert, *J. Catal.*, 2008, **259**, 96.
- 11 M. Iwasaki, K. Yamazaki, K. Banno and H. Shinjoh, *J. Catal.*, 2008, **260**, 205.
- 12 S. Brandenberger, O. Kröcher, A. Tissler and R. Althoff, *Appl. Catal., B*, 2010, **95**, 348.
- 13 M. Høj, M. J. Beier, J.-D. Grunwaldt and S. Dahl, *Appl. Catal., B*, 2009, **93**, 166.
- 14 D. Klukowski, P. Balle, B. Geiger, S. Wagloehner, S. Kureti, B. Kimmerle, A. Baiker and J. D. Grunwaldt, *Appl. Catal., B*, 2009, **93**, 185.

- 15 H. Sjövall, L. Olsson, E. Fridell and R. J. Blint, *Appl. Catal., B*, 2006, **64**, 180.
- 16 D. W. Fickel, E. D'Addio, J. A. Lauterbach and R. F. Lobo, *Appl. Catal., B*, 2011, **102**, 441.
- 17 S. J. Schmieg, S. H. Oh, C. H. Kim, D. B. Brown, J. H. Lee, C. H. F. Peden and D. H. Kim, *Catal. Today*, 2012, **184**, 252.
- 18 U. Deka, A. Juhin, E. A. Eilertsen, H. Emerich, M. A. Green, S. T. Korhonen, B. M. Weckhuysen and A. M. Beale, *J. Phys. Chem. C*, 2012, **116**, 4809.
- 19 P. G. W. A. Kompio, A. Brückner, F. Hipler, G. Auer, E. Löffler and W. Grünert, *J. Catal.*, 2012, **286**, 237.
- 20 Z. Si, D. Weng, X. Wu, J. Li and G. Li, *J. Catal.*, 2010, **271**, 43.
- 21 Z. Si, D. Weng, X. Wu, Y. Jiang and B. Wang, *Catal. Sci. Technol.*, 2011, **1**, 453.
- 22 L. Chen, J. Li, M. Ge and R. Zhu, *Catal. Today*, 2010, **153**, 77.
- 23 W. Shan, F. Liu, H. He, X. Shi and C. Zhang, *Chem. Commun.*, 2011, **47**, 8046.
- 24 F. Liu, H. He, Y. Ding and C. Zhang, *Appl. Catal., B*, 2009, **93**, 194.
- 25 M. Newville, *J. Synchrotron Radiat.*, 2001, **8**, 322.
- 26 J. J. W. Cook and D. E. Sayers, *J. Appl. Phys.*, 1981, **52**, 5024.
- 27 A. L. Ankudinov, B. Ravel, J. J. Rehr and S. D. Conradson, *Phys. Rev. B: Condens. Matter Mater. Phys.*, 1998, **58**, 7565.
- 28 W. S. Kijlstra, J. C. M. L. Daamen, J. M. van de Graaf, B. van der Linden, E. K. Poels and A. Bliëk, *Appl. Catal., B*, 1996, **7**, 337.
- 29 Z. Huang, Z. Liu, X. Zhang and Q. Liu, *Appl. Catal., B*, 2006, **63**, 260.
- 30 F. Liu and H. He, *Catal. Today*, 2010, **153**, 70.
- 31 J.-H. Park, H. J. Park, J. H. Baik, I.-S. Nam, C.-H. Shin, J.-H. Lee, B. K. Cho and S. H. Oh, *J. Catal.*, 2006, **240**, 47.
- 32 A. Sultana, T. Nanba, M. Haneda and H. Hamada, *Catal. Commun.*, 2009, **10**, 1859.
- 33 J. H. Kwak, R. G. Tonkyn, D. H. Kim, J. Szanyi and C. H. F. Peden, *J. Catal.*, 2010, **275**, 187.
- 34 J. H. Kwak, D. Tran, S. D. Burton, J. Szanyi, J. H. Lee and C. H. F. Peden, *J. Catal.*, 2012, **287**, 203.
- 35 G. Qi and R. T. Yang, *Appl. Catal., B*, 2003, **44**, 217.
- 36 T. Gao, P. Norby, F. Krumeich, H. Okamoto, R. Nesper and H. Fjellvåg, *J. Phys. Chem. C*, 2010, **114**, 922.
- 37 C. B. Azzoni, M. C. Mozzati, P. Galinetto, A. Paleari, V. Massarotti, D. Capsoni and M. Bini, *Solid State Commun.*, 1999, **112**, 375.
- 38 A. S. Mamede, E. Payen, P. Grange, G. Poncelet, A. Ion, M. Alifanti and V. I. Pârvulescu, *J. Catal.*, 2004, **223**, 1.
- 39 C. Santato, M. Odziemkowski, M. Ulmann and J. Augustynski, *J. Am. Chem. Soc.*, 2001, **123**, 10639.
- 40 S. S. Chan, I. E. Wachs, L. L. Murrell and N. C. Dispenziere Jr, *J. Catal.*, 1985, **92**, 1.
- 41 B. Thirupathi and P. G. Smirniotis, *Appl. Catal., B*, 2011, **110**, 195.
- 42 M. Kang, E. D. Park, J. M. Kim and J. E. Yie, *Appl. Catal., A*, 2007, **327**, 261.
- 43 G. Qi and R. T. Yang, *J. Phys. Chem. B*, 2004, **108**, 15738.
- 44 N.-Y. Topsøe, *Science*, 1994, **265**, 1217.
- 45 Z. Wu, B. Jiang, Y. Liu, H. Wang and R. Jin, *Environ. Sci. Technol.*, 2007, **41**, 5812.
- 46 L. Chen, J. Li and M. Ge, *Environ. Sci. Technol.*, 2010, **44**, 9590.
- 47 D. Sun, Q. Liu, Z. Liu, G. Gui and Z. Huang, *Catal. Lett.*, 2009, **132**, 122.
- 48 L. Chen, J. Li, M. Ge, L. Ma and H. Chang, *Chin. J. Catal.*, 2011, **32**, 836.
- 49 L. Liu, Y. Chen, L. Dong, J. Zhu, H. Wan, B. Liu, B. Zhao, H. Zhu, K. Sun, L. Dong and Y. Chen, *Appl. Catal., B*, 2009, **90**, 105.
- 50 F. Prinetto, M. Manzoli, S. Morandi, F. Frola, G. Ghiotti, L. Castoldi, L. Lietti and P. Forzatti, *J. Phys. Chem. C*, 2009, **114**, 1127.
- 51 M. Sirilumpen, R. T. Yang and N. Tharapiwattananon, *J. Mol. Catal. A: Chem.*, 1999, **137**, 273.
- 52 G. M. Underwood, T. M. Miller and V. H. Grassian, *J. Phys. Chem. A*, 1999, **103**, 6184.
- 53 B. Onida, F. Geobaldo, F. Testa, F. Crea and E. Garrone, *Microporous Mesoporous Mater.*, 1999, **30**, 119.
- 54 F. Liu, H. He, C. Zhang, W. Shan and X. Shi, *Catal. Today*, 2011, **175**, 18.
- 55 F. Liu and H. He, *J. Phys. Chem. C*, 2010, **114**, 16929.
- 56 A. Grossale, I. Nova, E. Tronconi, D. Chatterjee and M. Weibel, *J. Catal.*, 2008, **256**, 312.
- 57 G. Piazzesi, M. Elsener, O. Kröcher and A. Wokaun, *Appl. Catal., B*, 2006, **65**, 169.
- 58 G. Madia, M. Koebel, M. Elsener and A. Wokaun, *Ind. Eng. Chem. Res.*, 2002, **41**, 4008.
- 59 A. Grossale, I. Nova, E. Tronconi, D. Chatterjee and M. Weibel, *Top. Catal.*, 2009, **52**, 1837.
- 60 C. Ciardelli, I. Nova, E. Tronconi, D. Chatterjee and B. Bandl-Konrad, *Chem. Commun.*, 2004, 2718.
- 61 P. Forzatti, I. Nova and E. Tronconi, *Angew. Chem.*, 2009, **121**, 8516.